

# **UC Davis**

## **UC Davis Previously Published Works**

### **Title**

The effect of El Niño Southern Oscillation cycles on the decadal scale suspended sediment behavior of a coastal dry-summer subtropical catchment

### **Permalink**

<https://escholarship.org/uc/item/8mq449xr>

### **Journal**

Earth Surface Processes and Landforms, 40(2)

### **ISSN**

0197-9337

### **Authors**

Gray, Andrew B  
Pasternack, Gregory B  
Watson, Elizabeth B  
et al.

### **Publication Date**

2015-02-01

### **DOI**

10.1002/esp.3627

Peer reviewed

# **The effect of El Niño Southern Oscillation cycles on the decadal scale suspended sediment behavior of a coastal dry-summer subtropical catchment**

Andrew B. Gray<sup>a</sup>, Gregory B. Pasternack, Elizabeth B. Watson, Jonathan A. Warrick, and Miguel A. Goñi

<sup>a</sup> Corresponding author: Department of Land, Air and Water Resources, University of California, 1 Shields Ave., Davis, California 95616, USA , Tel: +01 530.752.1130, Fax: +01 530.752.5262, E-mail: abgray@ucdavis.edu

**Keywords:** suspended sediment, long term memory, El Niño Southern Oscillation, arid rivers, non-stationarity

## **Abstract**

Rivers display temporal dependence in suspended sediment – water discharge relationships. Although most work has focused on multi-decadal trends, river sediment behavior often displays sub-decadal scale fluctuations that have received little attention. The objectives of this study were to identify interannual to decadal scale fluctuations in the suspended sediment – discharge relationship of a dry-summer subtropical river, infer the mechanisms behind these fluctuations, and examine the role of El Niño Southern Oscillation climate cycles. The Salinas River (California) is a moderate sized ( $11,000 \text{ km}^2$ ), coastal dry-summer subtropical catchment with a mean discharge ( $Q_{mean}$ )

of  $11.6 \text{ m}^3\text{s}^{-1}$ . This watershed is located at the northern most extent of the for Pacific coastal North America region that experiences increased storm frequency during El Niño years. Event to interannual scale suspended sediment behavior in this system was known to be influenced by antecedent hydrologic conditions, whereby previous hydrologic activity regulates the suspended sediment concentration – water discharge relationship. Fine and sand suspended sediment in the lower Salinas River exhibited persistent, decadal scale periods of positive and negative discharge corrected concentrations. The decadal scale variability in suspended sediment behavior was influenced by interannual to decadal scale fluctuations in hydrologic characteristics, including: elapsed time since small ( $\sim 0.1x Q_{mean}$ ), and moderate ( $\sim 10x Q_{mean}$ ) threshold discharge values, the number of preceding days that low/no flow occurred, and annual water yield. El Niño climatic activity was found to have little effect on decadal-scale fluctuations in the fine suspended sediment – discharge relationship due to low or no effect on the frequency of moderate to low discharge magnitudes, annual precipitation, and water yield. However, sand concentrations generally increased in El Niño years due to the increased frequency of moderate to high magnitude discharge events, which generally increase sand supply.

## Introduction

Small to moderate sized basins ( $10\text{--}10^4 \text{ km}^2$ ) of high relief ( $> 2000 \text{ m}$ ) are known to export the majority of the terrestrial sediment flux to the oceans (Milliman and Syvitski, 1992). Most river sediment is transported in suspension (Walling, 1977), and

the relationship between suspended sediment concentration ( $C_{ss}$ ) and water discharge ( $Q$ ) is often highly variable in small systems (i.e. Bogen and Bonsnes, 2003; Farnsworth and Warrick, 2007). Furthermore, semi-arid rivers experiencing pronounced wet and dry seasons, such as the Salinas River of central California, often display particularly high variability in the  $C_{ss} - Q$  relationship (Warrick and Mertes, 2009; Farnsworth and Milliman, 2003; Gray et al., 2014).

Variability in the  $C_{ss} - Q$  relationship is determined by internal and external mechanisms that are highly dependent on temporal scale (Carson et al., 1973; Paustian and Beschta, 1979; Gao et al., 2007; Florsheim et al., 2011; Tote et al., 2011; Kuai and Tsai, 2012). Internal mechanisms are those that arise primarily from the characteristics of the basin, while external mechanisms stem primarily from environmental conditions exterior to the basin, such as climatic and solar forcings. Most estimations of decadal to multi-decadal suspended sediment flux assume stationarity in the  $C_{ss} - Q$  relationship and the mechanisms involved in its control (Helsel and Hirsch, 2002). Studies that have recognized temporal dependence in  $C_{ss} - Q$  focused on multi-decadal trends forced by long term anthropogenic activity or large disturbances such as wildfire or rare floods (i.e. Pasternack et al., 2001; Willis and Griggs, 2003; Walling, 2006; Warrick and Rubin, 2007; Warrick et al., 2012; Warrick et al., 2013). Conversely, studies focused on event scale forcings in small mountainous basins generally have not examined their effects on interannual or decadal scale patterns in suspended sediment behavior (i.e. Hudson, 2003; Lenzi and Marchi, 2000; Estrany et al., 2009; Mano et al., 2009).

Some mechanisms operate exclusively over a narrow temporal domain, and cease to influence systematic differences in suspended sediment concentrations as the

time period of comparison changes. For example, the event scale internal mechanism of differential peak  $C_{ss}$  and Q celerity downstream can lead to suspended sediment hysteresis – differing  $C_{ss}$  – Q relationships on the rising and falling limb of the hydrograph (Heidel, 1956; Marcus, 1989; Bull, 1997; Brasington and Richards, 2000). Differences in the average  $C_{ss}$  – Q relationship from one decade to the next would be unaffected by differences in peak  $C_{ss}$  and Q transit speeds. This would be the case even if systematic changes in sediment and discharge celerity occurred at the decadal scale, as long as the event integrated  $C_{ss}$  – Q relationship did not change.

However, event scale mechanisms can also affect longer term variation in suspended sediment behavior. One set of mechanisms for this temporal ‘up-scaling’ are the effects of antecedent basin conditions. The external factors of storm track location and precipitation intensity interact with the internal factors of basin ground cover and substrate characteristics to largely determine the delivery of water and sediment to the channel (Hicks et al., 2000; Ankers et al. 2003). The most commonly available record of these interactions over time is the discharge time series, which can in turn be used to describe the hydrologic preconditioning of the system (Hudson, 2003; Gray et al, 2014). Antecedent conditions can affect subsequent suspended sediment behavior by increasing or decreasing sediment supply, particularly in systems that experience seasonal and highly variable conditions at interannual and greater scales (i.e. Abraham, 1969; Hudson, 2003; Lana-Renault et al., 2007; Lana-Renault and Regues, 2009; Gray et al., 2014). Furthermore, event to seasonal scale land surface and channel disturbances can also play a large role in changing suspended sediment behavior over short temporal scales by altering sediment availability (i.e. Colby, 1956;

de Vente et al., 2007). Increased sediment availability in small to moderate sized basins has been observed after large floods in small mountainous basins (Abraham, 1969; Brown and Ritter 1971; Warrick et al., 2013). Flood events can also serve to flush semi-arid systems of sediment, exhausting sediment availability on an event basis or over the course of a storm season, which can have longer term effects on sediment supply (Hudson, 2003; Constantine et al., 2005; Batalla and Vericat, 2009; Gray et al., 2014).

In addition to the legacy effects of individual events,  $C_{ss} - Q$  relationships may also be steered by the seasonal, annual, or decadal scale patterns of persistent elevated or depressed hydrologic conditions. This is persistent dependency, or ‘long-term-memory’, wherein the previous states of a given parameter influences subsequent states over long time periods (Hurst, 1951; 1957). Discharge and transported constituent time series data from even relatively small basins ( $\sim 400 \text{ km}^2$ ) have displayed persistent dependency (Lawrence and Kottekoda, 1977; Montanari et al., 1997; Pelletier and Turcotte, 1997). Perhaps the most studied examples of decadal scale patterns in a fine scale are the external controls on suspended sediment exerted by the regional effects of climate cycles on sediment flux. El Niño Southern Oscillation (ENSO) and Pacific Decadal Oscillation (PDO) patterns have been shown to affect annual and event scale precipitation magnitudes/intensities, and influence water and suspended sediment discharge variability at annual and decadal scales along the northeastern Pacific coast (Inman and Jenkins, 1999; Farnsworth and Milliman, 2003; Andrews et al., 2004; Andrews and Atweiler, 2012). However, these studies focused on

the effects of climate cycles on discharge magnitude – frequency relationships applied to stationary  $C_{ss}$  – Q relationships.

This study directly addresses the assumption of a stationary suspended sediment – discharge relationship over multi-decadal time scales in the lower Salinas River, California. The central assertion is that decadal scale variability in the  $C_{ss}$  – Q relationship can be achieved through longer (interannual to decadal) temporal fluctuations or trends in the factors controlling event to annual scale suspended sediment behavior. The goals of this study were twofold. The first goal was to identify and describe the interannual to decadal scale patterns of suspended sediment – discharge behavior in the lower Salinas River, California. The second goal was to determine if interannual to decadal scale patterns in hydrologic conditions could explain the patterns observed in the  $C_{ss}$  – Q relationships. Event to annual scale hydrologic factors identified in previous work (Gray et al., 2014) were investigated for this purpose. The patterns in hydrologic factors were then examined in the context of regional climatic variability (ENSO cycling). Multi-decadal scale trends in suspended sediment behavior were then considered alongside trends in the discharge – precipitation relationship and in terms of decadal scale variability.

## **Study Region**

The Salinas River drains a ~11,000 km<sup>2</sup> portion of the Central Coast Ranges of California from a maximum relief of ~ 1,900 m. Mean discharge ( $Q_{mean}$ ) is 11.6 m<sup>3</sup>s<sup>-1</sup> through the lowest gauging station in the basin (USGS gauge #11152500: *Salinas*

*River near Spreckels*). This gauge and the next mainstem gauge 23.5 km upstream (USGS gauge # 11152300: *Salinas River near Chualar*,) are referred to in this study as S1 and S2, with drainage areas of 10,764 and 10,469 km<sup>2</sup>, respectively (Figure 1). The period of suspended sediment sampling between these two gauges spans 1967 to 2011, while discharge records extend from 1931 to present (USGS NWIS, 2013). The regional climate is dry-summer subtropical. Most annual precipitation originates from winter storms that occur from October through May, the largest of which are generally produced during strong El Niño years (Farnsworth and Milliman, 2003; Andrews et al., 2004). Geologic substrate is primarily Mesozoic sedimentary rock (Nutter, 1901; Rosenberg and Joseph, 2009). Land cover grades downslope from steep, forested headlands to chaparral and grassland assemblages in the lower hills, followed by lowlands that have been mostly converted to irrigation agriculture.

Agriculture is the largest anthropogenic disturbance in the Salinas River watershed in terms of area, followed by urbanization and dam emplacement (Thompson and Reynolds, 2002). Three major dams were constructed on the mainstem and two major eastern tributaries between 1941–1965 primarily for groundwater recharge purposes, motivated by irrigation demands that have led to overdrafting of Salinas aquifers since the early 20<sup>th</sup> century (Figure 1) (Thompson and Reynolds, 2002). Urbanization has increased significantly in the basin from 172 to 230 km<sup>2</sup> between 1984 and 2010, although this remains a relatively low proportion of basin area (~ 2%) (California Department of Conservation, 2013). Groundwater extraction, primarily for irrigated agriculture, and the return of a portion of these waters to the channel are a significant component of the hydrology of the Salinas River (Thompson and Reynolds,

2002). Irrigation agriculture intensity has increased since the 1960s, but irrigation water demands stabilized beginning in the 1990s due to the rapid rise of drip irrigation, which has largely supplanted less hydrologically efficient sprinkler and furrow methods (Thompson and Reynolds, 2002).

## Methods

This study focused on suspended sediment samples collected by Gray et al. (2014) and historical USGS samples from the lower Salinas River. Gray et al. (2014) collected 43 samples between water years 2008 and 2011 from bridges crossing the Salinas River at Davis Street (4 river km below S1) and the USGS gauging stations S1 and S2 (Figure 1). Water years begin on 1 October of the previous calendar year and end on 30 September of the calendar year. Samples were collected as per Warrick et al. (2012), with the following modifications. Samples were retrieved from the water surface at cross-channel stations of one-quarter, one-half, and three-quarters wetted channel width. Two 1-L samples from were collected from each cross-channel station for (i) total suspended sediment concentration ( $C_{ss}$ ) and (ii) particle size distribution analysis. One event was sampled at high resolution with 250-ml samples every 2 – 3 hours. Samples were measured volumetrically and then filtered through preweighed, combusted, Whatman GF/A, 0.7  $\mu\text{m}$  glass fiber filters. Filters were dried at 60°C for 24 h, cooled to room temperature under vacuum in a desiccator, and subsequently weighted to  $\pm 0.0001$  g. Sediment mass was obtained by subtracting filter mass from total mass. The  $C_{ss}$  was then calculated by dividing sediment mass by the initial

sample volume.

Particle size distribution analysis was performed on sediment recovered from water samples through centrifugation at 3250 g in 500-mL bottles for 10 min. Sediment was transferred to 150-mL beakers and treated with unheated and heated 30% H<sub>2</sub>O<sub>2</sub> aliquots to oxidize organic constituents. Organic free sediment was then dispersed with 0.5% sodium metaphosphate solution, and run through a Beckman-Coulter LS 230 (Beckman Coulter Inc., Fullerton, CA, USA) laser diffraction granulometer using polarization intensity differential scattering (PIDS) as per Gray et al. (2010).

Suspended sediment samples were collected from the surface of river flow. For this reason coarse suspended sediment particles were expected to be underrepresented. Sediment suspension calculations by particle size based on the characteristics of the highest and lowest flows showed that fine particles in the clay to silt range (diameter ( $D$ ) < 62.5 µm) should be uniformly distributed throughout the vertical profile (Rouse, 1937, 1938; Hill et al., 1988). Based on these estimations, analysis of the suspended sediment samples collected by the authors was restricted to fine particles of  $D$  < 62.5 µm. Values for fine suspended sediment concentration ( $C_{SSf}$ ) were calculated by multiplying  $C_{SS}$  by the proportion of sediment occurring in the fine fraction:

$$C_{SSf} = \frac{C_{SS} \times (\% \text{ particles} < 62.5 \mu\text{m})}{100} \quad (1)$$

The USGS collected flow-integrated  $C_{SS}$  samples from the Salinas River at locations corresponding to S1 and S2 from water years 1969 to 1986 and 1967 to 2010,

respectively (USGS NWIS, 2013). The 277 USGS samples used in this study represented a given discharge event and were associated with both instantaneous discharge and particle size data. The USGS samples were processed by sieving to establish the relative contribution of fine, and sand ( $2000 \mu\text{m} > D > 63.5 \mu\text{m}$ ) fractions. The  $C_{SSf}$  for these samples was calculated using Eq. (1), and the concentration of sand suspended sediment ( $C_{SSs}$ ) was obtained by subtracting  $C_{SSf}$  from  $C_{SS}$ . Hereafter, the term  $C_{SS}$  is used generally when referring to tests that were conducted separately on  $C_{SSf}$  and on  $C_{SSs}$ .

All suspended sediment data from the USGS were associated with instantaneous discharge values. Samples collected by the authors were assigned discharge values through linear interpolation between adjacent 15-min discharge data from the appropriate USGS gauge. Davis Street sample discharge was estimated from the S1 record of 15-min discharge data by applying a time lag to account for the transit of flow stage downstream. The time lag was computed from the estimated transit time ( $t_t$ ), where  $t_t$  was equal to the distance between Davis Street and S1 divided by the transit speed ( $\text{m s}^{-1}$ ) of peak flow between S2 and S1 for each discharge event in question. Transit speeds were found to be highly variable, ranging from 0.01 to  $2.38 \text{ m s}^{-1}$ , yet most values fell between 0.2 and  $0.8 \text{ m s}^{-1}$ . When the lagged time fell between 15-min discharge records, the associated discharge was calculated through linear interpolation.

Monthly precipitation ( $P$ ) data was obtained from the National Weather Service for the Big Sur State Park (BGS) gauge; the gauge that correlates most closely with lower Salinas River streamflow (Warrick et al., 2012; Gray et al., 2014). Historic El Niño activity was characterized in this study by (i) the Oceanic Niño Index (ONI), an

aggregate measurement of sea surface temperature defects from a 30 year base period average in the 5°N to 5°S by 120° to 170°W region and (ii) the extended Multivariate El Niño Index (MEI.ext), which incorporates the signals of several ENSO indices (Pedatella and Forbes, 2009; Wolter and Timlin, 2011). The National Oceanographic and Atmospheric Administration's (NOAA) three-month running average data for ONI were obtained for the interval of 1950 to 2011, while MEI.ext was retrieved from Wolter and Timlin (2011).

## **Computation and Data Analysis**

Rating curves were used in this study to represent bivariate relationships between environmental parameters for given periods of time. The residuals of these relationships were then used to describe changes in these relationships over time. Residuals were obtained by subtracting the expected value on each rating curve from observed sample values, in effect correcting sample  $C_{ss}$  or  $Wy$  for the influence of  $Q$  or  $P$ , respectively. The rating curves employed to individually model  $C_{ssf} \sim Q$ ,  $C_{sss} \sim Q$ , and annual water yield ( $Wy$ )  $\sim P$  relationships were constructed with simple linear regression and localized regression (LOESS) techniques applied to log-transformed data (Cleveland, 1979; Helsel and Hirsch, 2002; Gray et al., 2014). Suspended sediment rating curves were computed for the entire sediment sampling period (1967–2011), while  $Wy \sim P$  rating curves were calculated for the entire precipitation record (1930–2011) and just the 1967–2011 period. Rating curves were not corrected for log-

transform bias as back-transformation for flux estimation in original units was not conducted here.

Persistent patterns in suspended sediment behavior were identified by sequentially summing  $C_{SSf} \sim Q$  and  $C_{SSs} \sim Q$  LOESS residuals over time. This method, referred to hereafter as cumulative residual analysis, was first developed by Hurst in the 1950s for estimating reservoir storage requirements (Hurst 1951; 1957). Periods of persistent positive or negative behavior were identified based on the local slope of the cumulative residual curve, with persistent positive or negative values recognized by positive or negative slopes maintained over ranges of residual values  $\geq 3 \sigma$ , where  $\sigma$  is the standard deviation of the residuals.

Examination of persistent patterns in the hydrologic controls on suspended sediment behavior required variables representing these conditions. Gray et al. (2014) previously examined the effects of antecedent hydrologic conditions on suspended sediment behavior in the lower Salinas River. The significant hydrologic controls identified in that study were further examined here in terms of their decadal scale patterns of variability. The basic methodology of Gray et al. (2014) was to test for correlations between (i)  $C_{SSf} \sim Q$  or  $C_{SSs} \sim Q$  LOESS residuals and (ii) variables representing antecedent basin conditions using non-parametric Mann-Kendall analyses (Helsel and Hirsch, 2002). The following suites of variables were used to describe antecedent hydrologic conditions for each suspended sediment sample: (i)  $\Sigma Q_{0.1}$ : the sum of days when  $Q_d \leq 0.1 \text{ m}^3\text{s}^{-1}$  for back cast summation windows of 1 to 2000 days; (ii)  $Q_j \text{ Time}$ : a measurement of the amount of time that has elapsed since the last hydrologic event greater than or equal to a given magnitude ( $Q_j$ ). Additionally, *annual*

*water yield* for the current year was tested, as was  $\Delta Q_d$ , the change in daily discharge ( $Q_d$ ) from the day before sampling to the day of sampling.

The results of Gray et al. (2014) showed that  $C_{SSf} \sim Q$  LOESS residuals decreased with: (i) prolonged dry periods (increasing  $\Sigma Q_{0.1}$  with 1200 to 2000 day back cast summation windows), (ii) increased elapsed time since low discharge magnitudes ( $Q_j = \sim 1-4 \text{ m}^3\text{s}^{-1}$ ), and (iii) decreased elapsed time since moderate discharge magnitudes ( $Q_j = 100-200 \text{ m}^3\text{s}^{-1}$ ). Fine suspended sediment also displayed overall positive hysteresis (higher  $C_{SSf}$  concentrations on the rising limb of the hydrograph), which was reflected by a significant positive correlation with  $\Delta Q_d$ . In contrast,  $C_{SSs} \sim Q$  LOESS residuals decreased with: (i) seasonal to prolonged dry periods (increasing  $\Sigma Q_{0.1}$  with 10–2000 day back cast summation windows), and (ii) increasing elapsed time since a wide range of discharge magnitudes ( $Q_j = 1-1000 \text{ m}^3\text{s}^{-1}$ ), and increased with *annual water yield*.

Temporal patterns of the hydrologic conditions found by Gray et al. (2014) and the discharge time series were examined here to compare their decadal scale variability with that of fine, and sand suspended sediment. Individual variables were selected from the suites of  $\Sigma Q_{0.1}$  and  $Q_j$  *Time* variables that had been found to display significant correlations with suspended sediment behavior by Gray et al. (2014). The variables selected were those that produced the highest correlations. For fines the variable that produced the most negative correlation was  $Q_1$  *Time*, and the variables with the highest positive correlations were  $Q_{114}$  *Time*, and  $\Delta Q_d$ . The variables with the most negative correlations with sand were  $\Sigma Q_{0.1}$  with a 110 day sampling window, and  $Q_{400}$  *Time*. The variable with the highest positive correlations with sand were current *annual water yield*.

Persistence in descriptors of antecedent hydrologic conditions and the discharge time series was visualized by subtracting their mean values, and then sequentially summing these mean corrected values over time. These sequential sums of mean corrected hydrologic variable behaviors were compared to suspended sediment cumulative residual analysis results to assess the role hydrologic conditions in determining decadal scale patterns in suspended sediment behavior. The hydrograph of mean daily discharge values were also plotted to visualize the largest discharge events and longest droughts over the suspended sediment sampling record.

The role of ENSO was then investigated as a potential control on the hydrologic conditions found to influence suspended sediment behavior from 1950 to 2011. El Niño, or positive ENSO activity, has been associated with increased storm intensity in central to southern California region (Andrews and Antweiler, 2012). Previous studies have identified the Salinas basin as the northernmost of the central California rivers that respond to positive El Niño like conditions with an increased frequency of large P and Q events (Farnsworth and Milliman, 2003). To examine the coincidence of El Niño events and hydrologic event history of the lower Salinas River, plots of the annual sum of days with flows above threshold levels of 1, 100, 200 and 400  $\text{m}^3\text{s}^{-1}$ , and below 0.1  $\text{m}^3\text{s}^{-1}$  were compared to the three-month running mean ONI. To further examine the relationship between ENSO cycling and the discharge thresholds of interest, the annual sum of days satisfying the hydrologic criteria detailed above and annual P were plotted against annual peak ONI.

Finally, temporal trend analyses of ( $C_{ss} \sim Q$ ) or ( $W_y \sim P$ ) residuals were conducted using linear regression or Mann-Kendall methods to assess the multi-

decadal trajectory of  $C_{ss}$  and  $Wy$  changes in the basin. These approaches can be characterized as parametric (linear regression trends of linear regression residuals), mixed parametric/nonparametric (linear regression trends of LOESS residuals, or Mann-Kendall trends of linear regression residuals) or nonparametric (Mann-Kendall trends of LOESS residuals) (Helsel and Hirsch, 2002). All analyses were performed using R 3.0.1 with package “Kendall” (McLeod, 2011; R Development Core Team, 2013).

## Results

Linear and LOESS rating curves showed strong, generally linear relationships between  $Q$  and  $C_{ss}$  for  $Q > \sim 1 \text{ m}^3\text{s}^{-1}$ , with curved or flat tails for  $Q < \sim 1 \text{ m}^3\text{s}^{-1}$  (Figure 2a,b, Table 1). The  $R^2$  values for  $C_{ssf}$  and  $C_{sss}$  log linear rating curves were similar at 0.55 and 0.58, respectively, while the  $C_{ssf}$  slope was lower than that of  $C_{sss}$  (0.71 vs. 0.92), but with a  $\sim 2x$  higher offset (1.57 vs. 0.73). LOESS models accommodated this low  $Q$  curvature, which resulted in slightly lower RMSE values in comparison to log-linear regressions. Linear regression based  $Wy$  models also missed slight curvature in the response to  $P$ , which was slightly better described (e.g. resulted in lower RMSE values) by LOESS models for both temporal domains (Figure 2c,d). The LOESS curves were used for subsequent suspended sediment and water yield rating curve residual analysis, as this better fit resulted in less systematic bias with discharge.

Cumulative residual analysis revealed that Salinas River experienced periods of persistent higher-than-expected  $C_{ss}$  as well as the converse (Figure 3). Fine sediment displayed persistent periods of higher  $C_{ssf}$  from 1967–1979 and 1990–1993,

and persistent periods of lower  $C_{SSf}$  from 1980–1989 and 1994–2011 (Figure 3a). The latter period of lower  $C_{SSf}$  was characterized by a period of relatively constant values from about 2002 – 2009, followed by a rapid decline in values. Sand displayed persistent periods of higher  $C_{SSs}$  from 1967–1986, followed by a period of persistent lower  $C_{SSs}$  during 1987–2010 (Figure 3f). The period of persistent low sand concentrations was also characterized by a period of near constant values from about 1993 to 2005.

Plots of cumulative mean corrected values of the antecedent hydrologic condition descriptors revealed patterns in hydrologic history that may have played a role in decadal scale suspended sediment behavior (Figure 3b-d,g-i), with the hydrograph at S1 included for reference (Figure 3e,j). The most striking feature of these plots is a persistent dry period spanning the mid-1980s to early 1990s. Two hydrologic variables used to estimate fine sediment concentration,  $Q_1$  Time and  $Q_{114}$  Time, displayed very similar persistent behaviors over much of the sample period, with notable exceptions (Figure 3b,c). The cumulative residual results for  $Q_1$  Time showed displayed steady decreases in the mean corrected residual sums over periods from roughly 1966–1987 and 1993–2011, separated by a dramatic positive period that spanned the late 1980s to mid-1990s (Figure 3b). On the other hand,  $Q_{114}$  Time displayed constant values (with some variability) from 1965 – 1980 and 2000 – 2011, and persistent decreases from 1980 – 1990 and 1995 – 2000 (Figure 3c). The period of rapidly increasing mean corrected residual sums was also present for  $Q_{114}$  Time, but extended from the late 1980s to the early 1990s. The cumulative mean corrected plot for  $\Delta Q$  did not display persistent behavior, but rare large flood events did appear with their rapid, consecutive

increases in discharge magnitude, including the three largest peak events of the period of suspended sediment record, which occurred on 2/26/1969, 3/3/1983 and 3/12/1995 (Figure 3d,e).

The two hydrologic factors that negatively affected sand concentration calculations,  $\sum Q_{0.1}$  with a 110 day counting window, and  $Q_{400} \text{ Time}$ , also displayed a transition from persistent low to high values around the mid-1980s, with transition placement  $\sim$  1987 (Figure 3f,g). The behavior of  $\sum Q_{0.1}, 110 \text{ day}$  was generally stable after the end of the positive excursion ( $\sim$  1995), while  $Q_{400} \text{ Time}$  went through another cycle of persistent low (1995–2002) and high (2002–2011) values. *Current water yield*, the hydrologic factor that exerted a positive effect in the sand, exhibited a relatively stable period between 1967 and 1979, followed by a wetter period from 1979–1983, a prolonged dry period from 1983–1994, and brief wet interval from 1994–1998, and another prolonged dry period from 1998–2011 (Figure 3i).

In summary, the early portion of the suspended sediment record, from 1967 to mid-1980s, was characterized as hydraulically active with most days experiencing lower than average elapsed time since the last  $Q \geq 1, 114$ , and  $400 \text{ m}^3\text{s}^{-1}$ , and lower sums of previous very low to no flow days ( $Q \leq 0.1 \text{ m}^3\text{s}^{-1}$ ). Four of the six hydrologic events with peak  $Q > 1000 \text{ m}^3\text{s}^{-1}$  also occurred during this period (Figure 3e,j). This was followed by a very dry period that extended from the mid-1980s to the mid-1990s, with very little water flux through the lower Salinas River from 1988–1990 and no  $Q > 114 \text{ m}^3\text{s}^{-1}$  events until 1993. The period of the mid-1990s to present began with two large events, including the flood of 1995, which ushered in a short wet period that ended in the late 1990s, after which water yields and peak hydrologic events were generally low.

The period of persistent high fine sediment concentrations from 1967 to 1980 coincided with a period of persistently low  $Q_1$  *Time* values, and relatively constant  $Q_{400}$  *Time* values. Both periods of persistent low fine sediment concentration generally coincided with periods of persistent low  $Q_{114}$  *Time* values. The second period of low fine sediment concentration (1993–2011) also experienced a period of stable concentrations that coincided with a return to relatively constant  $Q_{114}$  *Time* values. However this period of stable concentration was followed by a return to persistent low concentrations, despite persistently low  $Q_1$  *Time* and stable  $Q_{114}$  *Time* values. The long dry interval spanning the late 1980s through the early 1990s lined up with the positive excursion of fine suspended sediment concentration in the early 1990s. This dry period also resulted in persistent increases in both  $Q_1$  *Time* and  $Q_{114}$  *Time* sums.

The mid-1980s transition to drought also marked the transition in persistent excess sand concentration from positive to negative. However, subsequent transitions to wetter periods did not result in a break in persistent negative sand concentrations, although a small, contemporaneous positive excursion was observed (Figure 3f).

The effects of ENSO activity on lower Salinas River discharge history were most evident for higher discharge events. Of 78 events with  $Q \geq 400 \text{ m}^3\text{s}^{-1}$  since 1950, 74 occurred during El Niño years, with most ( $n = 55$ ) occurring during stronger ( $\text{ONI} > 1$ ) El Niño years, including in 1969, 1983 and 1995 (Figures 4, 5a). Moderate flows ( $Q \geq 100$  and  $> 200 \text{ m}^3\text{s}^{-1}$ ) mostly occurred during El Niño years (Figures 4, 5b,c), while the number of days with  $Q_d \geq 1 \text{ m}^3\text{s}^{-1}$  and the sum of low flow ( $Q_d \leq 0.1 \text{ m}^3\text{s}^{-1}$ ) days as well as annual precipitation were insensitive to El Niño cycles (Figures 4, 5d,e,f). Of note is the fact that during many El Niño years the lower Salinas River did not experience any

high or moderate flows. Thus the El Niño cycle can be considered a condition of increased high flow frequency or risk. This is in agreement with Farnsworth and Milliman (2003), who found that stronger El Niño conditions led to increased likelihood of high discharge events, although ENSO indices were not linearly related to discharge magnitudes.

Monotonic temporal trends in ( $C_{SSf} \sim Q$ ) and ( $C_{SSs} \sim Q$ ) residuals from 1967–2011 were found to be negative for all four tests, with two-sided  $p$ -values well below 0.05 (Table 2, Figure 6). The  $Wy - P$  relationships for 1931–2011 and 1967–2011 showed decreasing trends, though most were not statistically significant (Table 2, Figure 7). The longer  $Wy - P$  dataset showed some indication of a decreasing trend in water yield, as the fully parametric test (linear regression of linear regression residuals) and the fully nonparametric test (Mann-Kendall analysis of LOESS residuals) yielded decreasing trends with  $p$  values slightly below 0.05 (Figure 7a). This was expected due to the emplacement of dams in the mid-20<sup>th</sup> century. None of the tests for temporal trends in the 1967–2011 subgroup of ( $Wy \sim P$ ) residuals showed temporal trends that were statistically significant (Figure 7b). Thus there was no significant multi-decadal scale change in the ( $Wy \sim P$ ) relationship over the period of suspended sediment record (1967 – 2011).

## Discussion

Persistent decadal scale fluctuations in positive and negative suspended sediment excursions from expected, discharge-controlled values occurred for fine and

sand fractions between water years 1967 and 2011. Decadal scale patterns in antecedent hydrologic conditions appeared to match the observed persistence in suspended sediment behavior in some cases, particularly for fines before the early-2000s and sand over the entire sample period. ENSO activity does not appear to be responsible for most of the antecedent hydrologic precondition characteristics that influence suspended sediment behavior, with the exception of increases in sand supply after larger events ( $Q > \sim 10x Q_{mean}$ ) and the flushing of fine sediment by moderate discharge events ( $10\text{--}20x Q_{mean}$ ). Slight decreasing multi-decadal trends in both fine and sand sediment behavior between 1967 and 2011 do not appear to have been affected by changes in the water yield – precipitation relationship.

Furthermore, no high discharge event triggers were found for interannual to decadal scale alterations in suspended sediment behavior. This was not surprising for fine sediment, as Gray et al. (2014) found no relationship between the timing of large discharge events and fine sediment behavior in the lower Salinas River. Recent large discharge events had been found to increase sand concentrations, but apparently these events did not lead to decadal scale shifts in sand behavior. Extreme flooding events have been shown to exert interannual to inter-decadal effects on suspended sediment behavior in other river systems (Syvitski et al., 2000; Smith et al., 2003; Warrick et al., 2013). For example, Warrick et al. (2013) found that the large 1965 floods resulted in very high  $C_{ss}$  states in northern California rivers and that these states decayed for years thereafter, leading to inter-decadal, negative trends in  $C_{ss}$  residuals. Other systems have also shown this decaying sediment augmentation associated with extreme events (e.g. Morehead et al., 2003). These effects are often found in systems with large tracts

of steep, unstable hillslopes prone to mass wasting (Korup, 2012), such as the Eel River of Northern California (Brown and Ritter et al., 1971). In these cases, large, high-intensity precipitation events can speed up existing slides, trigger new slides, and initiate or expand gully style drainage of the resulting land surface scars, while high river discharge can truncate landslide snouts that reach the valley floor and cause further increases in downslope transport of sediment (Kelsey, 1980). In contrast, the Salinas basin is underlain by more stable bedrock and is not subject to the level of mass wasting found in the Eel River watershed (Nutter, 1901).

The lack of evidence for persistent effects of large floods on sediment behavior in the lower Salinas River may also be due to the fact that no ‘extreme’ events were captured during the period of suspended sediment sampling. The two largest hydrologic events during 1967–2011 occurred in 1969 and 1995 and produced peak discharges on the order of  $1800 \text{ m}^3\text{s}^{-1}$ , which translates to a return period of only  $\sim 20$  years. In contrast, the 1964 event on the Eel River was estimated to be a 200–400 year flood (Brown and Ritter, 1971; Sloan et al. 2001). Although sediment concentrations were generally high in the lower Salinas River after the 1969 event, they were also high for the few years sampled before it, while the 1995 event was in a period of low  $C_{ss}$ , which did not appear to be altered by the passing of this moderately large flood (see Figure 4).

More moderate discharge magnitudes appear to have a larger bearing on decadal scale suspended sediment behavior than floods in the lower Salinas River. Time series of more moderate in-channel flows experienced by the Salinas River expressed persistent behavior over time scales similar to that of suspended sediment

(i.e. interannual to decadal, see Figure 4). These flow magnitudes have been shown to exert statistically significant effects on suspended sediment behavior (Gray et al., 2014). Indeed, decadal scale patterns in hydrologic variable states seemed to reveal a simple and consistent underpinning for the patterns in sand behavior (see Figure 3). Wetter conditions prevailed in the early part of the record (late 1960s to mid-1980s), which led to persistent low values in hydrologic variables shown to have negative effects on  $C_{SSs}$ , and relatively stable to positive values for variables shown to have positive effects. This temporal zone coincides with that of high sand concentrations, which supports the notion that hydrologic preconditions could be the major factor controlling the behavior of  $C_{SSs}$ . A shift to dry conditions around the mid-1980s led to generally high values in variables with ‘negative’ forcing, and low values of variables with ‘positive’ forcing. This coincides with the onset of the negative period of sand sediment behavior, which ran from the mid-1980s to the end of sampling in 2010. A short wet period in the late 1990s also coincides with a minor period of positive sand activity in this otherwise negative period. Thus, interannual to decadal scale patterns in sand behavior seems to be controlled in part by decadal scale basin wetness and the frequency of moderate to large hydrologic events.

The relationship between fine suspended sediment and hydrologic preconditions was more complicated, but also generally consistent (see Figure 3). The two hydrologic variables that expressed decadal scale persistence,  $Q_1$  Time, which decreases  $C_{SSf}$  through time, and  $Q_{114}$  Time, which increases  $C_{SSf}$  through time (Gray et al., 2014), follow similar patterns of persistent deviation from their respective mean states. The third variable used in this study,  $\Delta Q_d$ , operated at the event scale and did not exhibit

interannual or decadal scale persistent behavior. In this case the decadal scale variability in fine sediment behavior seems to display a distinct sensitivity to  $Q_{114}$  *Time* rather than  $Q_1$  *Time*. Persistent periods of low  $Q_{114}$  *Time* generally coincided with periods of low fine sediment concentration, while stable or high values of  $Q_{114}$  *Time* generally coincided with periods of stable or high fine sediment concentration. In contrast, shifts in fine sediment behavior do not appear to be sensitive to the persistent patterns of the negative controls exerted by  $Q_1$  *Time*. Thus, depletion of subsequent fine sediment concentrations by moderate ( $100\text{--}200 \text{ m}^3\text{s}^{-1}$ ) ‘flushing’ flows, appears to exert a larger control on the decadal scale behavior of fine sediment than the timing of very low ( $1$  to  $4 \text{ m}^3\text{s}^{-1}$ ) flows. However, a notable discrepancy is apparent at the end of the record, as persistent low fine sediment concentrations continue despite stable  $Q_{114}$  *Time* values.

But how do flows of these low to moderate magnitudes respond to regional climate controls? The large infrequent flood events ( $Q \geq 40x Q_{mean}$ ) that transport the majority of the sediment through the Salinas River (Farnsworth and Milliman, 2003) occur almost exclusively during El Niño years (see Figure 6). Short elapsed time, from days to years, since the last moderate to high discharge event has been shown to increase sand concentrations in the lower Salinas River (Gray et al, 2014). In contrast, this study found that moderate  $Q$  peaks ( $100\text{--}200 \text{ m}^3\text{s}^{-1}$ , or  $\sim 10\text{--}20 Q_{mean}$ ), which act as a flushing function on fine suspended sediment supplies, were only slightly influenced by El Niño activity. This finding contrasts with other systems bearing marked wet/dry seasonality interacting with decadal scale ENSO cycles, such as the Puyango-Tumbes River of Ecuador, which was found to experience significant flushing of

channel-mediated sediments at seasonal as well as decadal scale wet conditions associated with El Niño events (Tarras-Wahlberg and Lane, 2003). Furthermore, neither total precipitation nor low flow days in the Salinas River Basin were influenced by El Niño. Therefore, ENSO cycles appear to increase total  $C_{SS}$  by augmenting sand sediment supply due to closer timing of high peak Q's, while fine suspended sediment behavior remains relatively insensitive to ENSO cycles. This finding suggests that ENSO cycles lead to increases in suspended sediment flux through increased frequency of high discharge events that move much of the sediment through the Salinas Basin (Farnsworth and Milliman, 2003; Wheatcroft et al., 2010). Furthermore, ENSO cycles enhance this effect by augmenting sand rating curves.

Slightly negative, multi-decadal trends in both fines and sand were found over the period of record (see Figure 7). Decadal scale patterns in behavior are implicated in these longer scale trends, as the sampling period began with positive, and ended with negative zones of persistent behavior for both texture classes. Multi-decadal trends in suspended sediment behavior are often attributed to anthropogenic changes to the land surface (Kallache et al., 2005; Walling, 2006), including urbanization (Espey, 1969; Hollis, 1975; Trimble, 1997; Warrick and Rubin, 2007), agricultural practices (Walling and Fang, 2003; McHugh et al., 2008; Deasy et al., 2009), and channel modification (Vorosmarty et al., 2003; Willis and Griggs, 2003). Very little change in proportional urban area has occurred in the Salinas basin (California Department of Conservation, 2013), and the major damming projects of the upper Salinas River mainstem and tributaries were already in place years before the initiation of sediment monitoring (SRCMP, 2009). Furthermore, no significant change was observed in the relationship

between precipitation and discharge from 1967 – 2011 (see Figure 7), which is one of the major mechanisms related to changing sediment – discharge behavior with urbanization and channel modification (Willis and Griggs, 2003; Warrick and Rubin, 2007).

However, agricultural intensity increased over this period and irrigation practices shifted from sprinkler and furrow to drip irrigation (Monterey County, 2013). This change in agricultural technology may have contributed to the negative trends in suspended sediment concentration, and the prolonged negative zone of fine sediment behavior from the mid-1990s to 2011. Wildfire may also be at play, as Warrick et al. (2012) found that sediment flux from the Arroyo Seco, a major subbasin of the Salinas River, was highly controlled by wildfire and large precipitation event sequences. Further investigation would be required to explicitly link agricultural practices and wildfire activity to the suspended sediment behavior patterns observed here.

## Conclusions

The lower Salinas River displayed decadal scale persistence in the suspended sediment – discharge behavior of fine and sand sized suspended sediment. Fine sediment displayed two couplets of alternating positive/negative periods of behavior, while sand exhibited only one positive and one negative period.

These patterns of suspended sediment behavior appear to have been caused in part by decadal scale persistence in hydrologic conditions. The initial positive periods of both fine and sand behavior occurred during a hydrologically active period when low to

moderate discharge events were frequent (1967 – 1980). Sand transitioned to its negative period with the transition to less hydrologically active conditions, and has remained in this state through the rest of the record. Transitions between positive and negative periods of persistent fine sediment behavior were consistently correlated with persistent patterns in the positive effect of longer elapsed time since moderate ( $\sim 10x Q_{mean}$ ) flows. This generally swamped out the negative effects on fine sediment concentration exerted by longer elapsed times since very low ( $\sim 1/10x Q_{mean}$ ) flows. This suggests that a flushing function associated with moderate discharges ( $10\text{--}20x Q_{mean}$ ) is a dominant control on interannual to decadal scale fine sediment behavior in the lower Salinas River.

A minimal effect was found for ENSO cycles on these hydrologic conditions, and by extension suspended sediment behavior at decadal scales. Positive ENSO periods led to increases in the frequency of moderate to large events, with an increase in effect found between moderate ( $Q = 10 - 20x Q_{mean}$ ) and large ( $Q \geq 40x Q_{mean}$ ) events. The lack of effect on drought/small discharge magnitude frequency and weak control on moderate discharge frequency suggests that ENSO plays a small role in modulating decadal scale fine sediment behavior. However, increased sand concentration due to large discharge events suggested that positive ENSO phases do augment sand concentration.

Finally, inconsistencies in decadal scale behavior of fine sediment vis-à-vis hydrologic conditions implied that additional, unstudied factors are at play. This notion is supported in part by overall negative trend in both fine and sand suspended sediment concentrations. Future mechanistic studies of landscape forcing factors are required to

address this issue, with particular regard to agricultural practices – the largest anthropogenic influence in the basin.

### **Acknowledgements**

This research was funded largely by the National Science Foundation under award No. 0628385 and secondarily by the Hydrologic Sciences Graduate Group at the University of California at Davis. This project was also supported by the USDA National Institute of Food and Agriculture, Hatch project number #CA-D-LAW-7034-H. Any opinions, findings and conclusions or recommendations expressed in this material are those of the authors and do not necessarily reflect the views of the National Science Foundation. We thank Peter Barnes, Sarah Greve, Duyen Ho, Olivia Oseguera, Larissa Salaki, and the Elkhorn Slough National Estuarine Research Reserve for laboratory and field assistance, and Rocko Brown for valuable discussion.

### **References**

Abraham CE. 1969. Suspended sediment discharges in streams. U.S. Army Corps of Engineers. Hydrologic Engineering Center. Davis, CA. Technical Paper 19, 10 pp.

Andrews ED, Antweiler RC. 2012. Sediment Fluxes from California Coastal Rivers: The Influences of Climate, Geology, and Topography. *Journal of Geology* **120**: 349-366.

Andrews ED, Antweiler RC, Neiman PJ, Ralph FM. 2004. Influence of ENSO on flood frequency along the California coast. *Journal of Climate* **17**: 337-348.

Ankers C, Walling DE, Smith RP. 2003. The influence of catchment characteristics on suspended sediment properties. *Hydrobiologia* **494**: 159-167.

Batalla RJ, Vericat D. 2009. Hydrological and sediment transport dynamics of flushing flows: implications for management in large Mediterranean rivers. *River Research and Applications* **25**: 297-314.

Bogen J, Bonsnes TE. 2003. Erosion and sediment transport in High Arctic rivers, Svalbard. *Polar Research* **22**: 175-189. DOI: 10.1111/j.1751-8369.2003.tb00106.x.

Brasington J, Richards K. 2000. Turbidity and suspended sediment dynamics in small catchments in the Nepal Middle Hills. *Hydrological Processes* **14**: 2559-2574.

Brown WM, Ritter JR. 1971. Sediment transport and turbidity in the Eel River Basin, California: U.S. Geological Survey Water-Supply Paper 1986, 67pp.

Bull LJ. 1997. Relative velocities of discharge and sediment waves for the River Severn, UK. *Hydrological Sciences Journal-Journal Des Sciences Hydrologiques* **42**: 649-660.

California Department of Conservation. 2013. Monterey County land use data. (last accessed 12/2013) <http://www.conservation.ca.gov/Index/Pages/Index.aspx>.

Carson MA, Taylor CH, Grey BJ. 1973. Sediment production in a small Appalachian watershed during spring runoff - Eaton-Basin, 1970-1972. *Canadian Journal of Earth Sciences* **10**: 1707-1734.

Cleveland WS. 1979. Robust locally weighted regression and smoothing scatterplots. *J. Am. Stat. Assoc.* **74**: 829-836.

Colby BR. 1956. Relationship of sediment discharge to streamflow. U.S. Geological Survey. Reston, VA. Open file report. 170 pp.

Constantine JA, Pasternack GB, Johnson ML. 2005. Logging effects on sediment flux observed in a pollen-based record of overbank deposition in a northern California catchment. *Earth Surface Processes and Landforms* **30**: 813-821.

de Vente J, Poesen J, Arabkhedri M, Verstraeten G. 2007. The sediment delivery problem revisited. *Progress in Physical Geography* **31**: 155-178.

Deasy C, Brazier RE, Heathwaite AL, Hodgkinson R. 2009. Pathways of runoff and sediment transfer in small agricultural catchments. *Hydrological Processes* **23**: 1349-1358.

Estrany J, Garcia C, Batalla RJ. 2009. Suspended sediment transport in a small Mediterranean agricultural catchment. *Earth Surface Processes and Landforms* **34**: 929-940. DOI: 10.1002/esp.1777.

Espey WH. 1969. Urban effects on the unit hydrograph. Effects of watershed changes on streamflow (Moore, W. L. and Morgan, C. W., eds.), University of Texas Press, Austin. 215-228.

Farnsworth KL, Milliman JD. 2003. Effects of climatic and anthropogenic change on small mountainous rivers: the Salinas River example. *Global and Planetary Change* **39**: 53-64.

Farnsworth, KL, Warrick, JA. 2007. Sources, Dispersal, and Fate of Fine Sediment Supplied to Coastal California. U.S. Geological Survey Scientific Investigations Report 2007-5254, Washington, D.C., 77pp.

Florsheim JL, Pellerin BA, Oh NH, Ohara N, Bachand PAM, Bachand SM, Bergamaschi BA, Hernes PJ, Kavvas ML. 2011. From deposition to erosion: Spatial and temporal variability of sediment sources, storage, and transport in a small agricultural watershed. *Geomorphology* **132**: 272-286. DOI: 10.1016/j.geomorph.2011.04.037.

Gao P, Pasternack GB, Bali KM, Wallender WW. 2007. Suspended-sediment transport in an intensively cultivated watershed in southeastern California. *Catena* **69**: 239-252.  
DOI: 10.1016/j.catena.2006.06.002.

Gray AB, Pasternack GB, Watson EB. 2010. Hydrogen peroxide treatment effects on the particle size distribution of alluvial and marsh sediments. *Holocene* **20**: 293-301.

Gray AB, Warrick JA, Pasternack GB, Watson EB, Goñi MA. 2014. Suspended sediment behavior in a coastal dry-summer subtropical catchment: effects of hydrologic preconditions. *Geomorphology* **214**: 485-501.

Heidel SG. 1956. The progressive lag of sediment concentration with flood waves. *Trans. Am. Geoph. Union.* **31**: 56-66.

Helsel DR, Hirsch RM. 2002. Statistical methods in water resources—hydrologic analysis and interpretation: U.S. Geological Survey Techniques of Water-Resources Investigations. 510 pp.

Hicks DM, Gomez B, Trustrum NA. 2000. Erosion thresholds and suspended sediment yields, Waipaoa River Basin, New Zealand. *Water Resour. Res.* **36**: 1129-1142.

Hill PS, Nowell ARM, Jumars PA. 1988. Flume evaluation of the relationship between suspended sediment concentration and excess boundary shear-stress. *Journal of Geophysical Research-Oceans* **93**: 12499-12509. DOI: 10.1029/JC093iC10p12499.

Hollis GE. 1975. The effect of urbanization on floods of different recurrence interval. *Water Resour. Res.* **11**: 431-434.

Hudson PF. 2003. Event sequence and sediment exhaustion in the lower Panuco Basin, Mexico. *Catena* **52**: 57-76.

Hurst HE. 1951. Long-term storage capacity of reservoirs. *Transactions of the American Society of Civil Engineers* **116**: 770-799.

Hurst HE. 1957. Suggested statistical model of some time series which occur in nature. *Nature* **180**: 494-494.

Inman DL, Jenkins SA. 1999. Climate change and the episodicity of sediment flux of small California rivers. *Journal of Geology* **107**: 251-270.

Kallache M, Rust HW, Kropp J. 2005. Trend assessment: applications for hydrology and climate research. *Nonlin. Proc. in Geophys.* **12**: 201-210.

Kelsey HM. 1980. A sediment budget and an analysis of geomorphic process in the Van-Duzen river basin, north coastal California, 1941-1975 - summary. *Geological Society of America Bulletin* **91**: 190-195.

Korup O. 2012. Earth's portfolio of extreme sediment transport events. *Earth-Science Reviews* **112**: 115-125.

Kuai KZ, Tsai CW. 2012. Identification of varying time scales in sediment transport using the Hilbert-Huang Transform method. *Journal of Hydrology* **420**: 245-254. DOI: 10.1016/j.jhydrol.2011.12.007.

Lana-Renault N, Regues D. 2009. Seasonal patterns of suspended sediment transport in an abandoned farmland catchment in the Central Spanish Pyrenees. *Earth Surface Processes and Landforms* **34**: 1291-1301.

Lana-Renault N, Regues D, Marti-Bono C, Begueria S, Latron J, Nadal E, Serrano P, Garcia-Ruiz JM. 2007. Temporal variability in the relationships between precipitation, discharge and suspended sediment concentration in a small Mediterranean mountain catchment. *Nordic Hydrology* **38**: 139-150.

Lawrence A, Kottekoda N. 1977. Stochastic modelling of river-flow time series, *J. R. Stat. Soc.* **140**: 1-47.

Lenzi MA, Marchi L. 2000. Suspended sediment load during floods in a small stream of the Dolomites (northeastern Italy). *Catena* **39**: 267-282.

Mano V, Nemery J, Belleudy P, Poirel A. 2009. Assessment of suspended sediment transport in four alpine watersheds (France): influence of the climatic regime. *Hydrological Processes* **23**: 777-792.

Marcus WA. 1989. Lag-time routing of suspended sediment concentrations during unsteady-flow. *Geological Society of America Bulletin* **101**: 644-651. DOI: 10.1130/0016-7606(1989)101<0644:ltross>2.3.co;2.

McHugh AD, Bhattacharai S, Lotz G, Midmore DJ. 2008. Effects of subsurface drip irrigation rates and furrow irrigation for cotton grown on a vertisol on off-site movement of sediments, nutrients and pesticides. *Agronomy for Sustainable Development* **28**: 507-519.

McLeod AI. 2011. Package 'Kendall.' Kendall rank correlation and Mann-Kendall trend test. CRAN. Classification/MSC 62M10, 91B84. <http://www.stats.uwo.ca/faculty/aim>. (last accessed: 10/2013).

Milliman JD, Syvitski JPM. 1992. Geomorphic/tectonic control of sediment discharge to the ocean: the importance of small mountainous rivers. *Journal of Geology* **100**: 525-544.

Montanari A, Rosso R, Taqqu M. 1997. Fractionally differenced ARIMA models applied to hydrologic time series: Identification, estimation and simulation. *Water Resour. Res.* **33**: 1035-1044.

Monterey County Agricultural Commissioner's Office Crop Reports. 2013.  
<http://ag.co.monterey.ca.us/resources/category/crop-reports> (last accessed 12/2013)

Morehead MD, Syvitski JP, Hutton EWH, Peckham SD. 2003. Modeling the temporal variability in the flux of sediment from ungauged river basins. *Global and Planetary Change* **39**: 95-110.

Nutter EH. 1901. Sketch of the geology of the Salinas Valley, California. *Journal of Geology*. **9**: 330-336.

Pasternack GB, Brush GS, Hilgartner WB. 2001. Impact of historic land-use change on sediment delivery to a Chesapeake Bay subestuarine delta. *Earth Surface Processes and Landforms* **26**: 409-427.

Paustian SJ, Beschta RL. 1979. Suspended sediment regime of an Oregon Coast Range stream. *Water Resources Bulletin* **15**: 144-154.

Pedatella NM, Forbes JM. 2009. Interannual variability in the longitudinal structure of the low-latitude ionosphere due to the El Nino-Southern Oscillation. *Journal of Geophysical Research-Space Physics* **114**: A12316.

Pelletier JD, Turcotte DL. 1997. Long-range persistence in climatological and hydrological time series: analysis, modeling and application to drought hazard assessment. *Journal of Hydrology* **203**: 198-208.

R Development Core Team. 2013. R: A language and environment for statistical computing. R Foundation for Statistical Computing, Vienna, Austria. <http://www.R-project.org/> (last accessed: 10/2013).

Rosenberg LI. and Joseph JC. 2009. Map of the Rinconada and Reliz Fault Zones, Salinas River Valley, California: U.S. Geological Survey Scientific Investigations Map 3059, scale 1:250,000 with pamphlet URL <http://pubs.usgs.gov/sim/3059/>.

Rouse H. 1937. Modern conceptions of the mechanics of fluid turbulence. *Transactions of the American Society of Civil Engineers* **102**: 463–541.

Rouse H. 1938. Fluid mechanics for hydraulic engineers, Dover, New York, 422 pp.

Sloan J, Miller JR, Lancaster N. 2001. Response and recovery of the Eel River, California, and its tributaries to floods in 1955, 1964, and 1997. *Geomorphology* **36**: 129-154.

Smith BPG, Naden PS, Leeks GJL, Wass PD. 2003. The influence of storm events on fine sediment transport, erosion and deposition within a reach of the River Swale, Yorkshire, UK. *Science of the Total Environment* **314**: 451-474.

SRCMP (Salinas River Channel Maintenance Program). 2009. Monterey County Water Resources Agency. 81pp.

Syvitski JP, Morehead MD, Bahr DB, Mulder T. 2000. Estimating fluvial sediment transport: The rating parameters. *Water Resour. Res.* **36**: 2747-2760.

Tarras-Wahlberg NH, Lane SN. 2003. Suspended sediment yield and metal contamination in a river catchment affected by El Nino events and gold mining activities: the Puyango river basin, southern Ecuador. *Hydrological Processes* **17**: 3101-3123.  
DOI: 10.1002/hyp.1297

Thompson JG, Reynolds R. 2002. Cultural evolution and water management in the Salinas River Valley. *Journal of the American Water Resources Association* **38**: 1661-1677.

Tote C, Govers G, Van Kerckhoven S, Filiberto I, Verstraeten G, Eerens H. 2011. Effect of ENSO events on sediment production in a large coastal basin in northern Peru. *Earth Surface Processes and Landforms* **36**: 1776-1788. DOI: 10.1002/esp.2200.

Trimble SW. 1997. Contribution of stream channel erosion to sediment yield from an urbanizing watershed. *Science* **278**: 1442-1444.

U.S. Geological Survey National Water Information System (USGS NWIS). 2013  
<http://waterdata.usgs.gov/nwis/sw> (last accessed: 03/2013).

Verosmarty CJ, Meybeck M, Fekete B, Sharma K, Green P, Syvitski JPM. 2003. Anthropogenic sediment retention: major global impact from registered river impoundments. *Global and Planetary Change* **39**: 169-190.

Walling DE. 1977. Assessing accuracy of suspended sediment rating curves for a small basin. *Water Resour. Res.* **13**: 530-538.

Walling DE. 2006. Human impact on land-ocean sediment transfer by the world's rivers. *Geomorphology* **79**: 192-216.

Walling DE, Fang D. 2003. Recent trends in the suspended sediment loads of the world's rivers. *Global and Planetary Change* **39**: 111-126.

Warrick JA, Mertes LAK. 2009. Sediment yield from the tectonically active semiarid Western Transverse Ranges of California. *Geol. Soc. Am. Bull.* **121**: 1054-1070.

Warrick JA, Rubin DM. 2007. Suspended-sediment rating curve response to urbanization and wildfire, Santa Ana River, California. *Journal of Geophysical Research-Earth Surface* **112**. DOI: F0201810.1029/2006jf000662.

Warrick JA, Hatten JA, Pasternack GB, Gray AB, Goni MA, Wheatcroft RA. 2012. The effects of wildfire on the sediment yield of a coastal California watershed. *Geological Society of America Bulletin* **124**: 1130-1146. DOI: 10.1130/b30451.1.

Warrick JA, Madej MA, Goni MA, Wheatcroft RA. 2013. Trends in the suspended-sediment yields of coastal rivers of northern California, 1955-2010. *Journal of Hydrology* **489**: 108-123. DOI: 10.1016/j.jhydrol.2013.02.041.

Wheatcroft RA, Goni MA, Hatten JA, Pasternack GB, Warrick JA. 2010. The role of effective discharge in the ocean delivery of particulate organic carbon by small, mountainous river systems. *Limnology and Oceanography* **55**: 161-171. DOI: 10.4319/lo.2010.55.1.0161.

Willis CM, Griggs GB. 2003. Reductions in fluvial sediment discharge by coastal dams in California and implications for beach sustainability. *Journal of Geology* **111**: 167-182.

Wolter K, Timlin MS. 2011. El Nino/Southern Oscillation behaviour since 1871 as diagnosed in an extended multivariate ENSO index (MEI.ext). *International Journal of Climatology* **31**: 1074-1087. DOI: 10.1002/joc.2336.

**Table 1: Suspended Sediment Rating Curves****Suspended Sediment Concentration ~ Water Discharge Linear Regression and LOESS Rating Curves**

Sediment Size	Temporal Zone <sup>a</sup>	Model	Model Equation	R <sup>2</sup>	RMSE <sup>b</sup>
Fine	Total Range (1967 - 2011)	Linear Regression	$\log C_{SS} = 1.569 + 0.713 * \log Q$	0.55	0.61
		LOESS	-	-	0.59
	1967 - 1979	Linear Regression	$\log C_{SS} = 1.896 + 0.634 * \log Q$	0.56	0.57
		LOESS	-	-	0.56
	1980 - 89, 1994 - 2011	Linear Regression	$\log C_{SS} = 1.326 + 0.651 * \log Q$	0.6	0.43
		LOESS	-	-	0.42
	1990 - 1993	Linear Regression	$\log C_{SS} = 2.233 + 0.850 * \log Q$	0.45	0.78
		LOESS	-	-	0.81
	Total Range (1967 - 2010)	Linear Regression	$\log C_{SS} = 0.726 + 0.920 * \log Q$	0.69	0.60
		LOESS	-	-	0.55
Sand	1967 - 1986	Linear Regression	$\log C_{SS} = 0.670 + 0.947 * \log Q$	0.70	0.60
		LOESS	-	-	0.52
	1987 - 2010	Linear Regression	$\log C_{SS} = 0.228 + 1.125 * \log Q$	0.71	0.53
		LOESS	-	-	0.48

**Annual Water Yield<sup>c</sup> ~ Precipitation<sup>d</sup> Linear Regression and LOESS Rating Curves**

Dependent Var.	Temporal Zone <sup>a</sup>	Model	Model Equation	R <sup>2</sup>	RMSE <sup>b</sup>
Water Yield	Total Range (1931 - 2011)	Linear Regression	$\log Wy = 5.11 * \log P - 8.22$	0.75	0.45
		LOESS	-	-	0.42
Water Yield	1967 - 2011	Linear Regression	$\log Wy = 4.93 * \log P - 7.90$	0.79	0.42
		LOESS	-	-	0.41

<sup>a</sup>All years reported as water years, beginning on October 1 of the previous year and running through September 30 of indicated year.

<sup>b</sup>Indicates root mean squared error (RMSE) values for the entire model. All RMSE values reported in log units.

<sup>c</sup>Annual water yield in units of 10<sup>5</sup> m<sup>3</sup> at USGS station 'Salinas River near Spreckles' ID# 11152500, referred to here as 'S1'.

<sup>d</sup>Annual precipitation in units of cm from NOAA gauge 'Big Sur State Park' (BGS).

**Table 2.** Temporal Trends

Temporal Range	Relationship	Test	Kendall tau	Kendall P-value	LR Coeff.	LR R <sup>2</sup>	LR P-value
1967-2011	Fine Sediment ( $C_{SSf} \sim Q$ )	LR residuals	-0.23	2.3E-10	-3.0E-05	0.09	5.0E-08
1967-2011		LOESS residuals	-0.20	1.7E-07	-3.0E-05	0.06	5.9E-06
1967-2010	Sand ( $C_{SSs} \sim Q$ )	LR residuals	-0.22	5.7E-08	-5.0E-05	0.11	3.2E-08
1967-2010		LOESS residuals	-0.14	6.3E-04	3.1E-05	0.050	1.8E-04
1931-2011	$Wy \sim P$	LR residuals	-0.03	0.72	-4.2E-03	0.05	0.05
1931-2011		LOESS residuals	-0.18	0.02	-3.4E-03	0.04	0.09
1967-2011		LR residuals	-0.10	0.34	-4.9E-03	0.03	0.32
1967-2011		LOESS residuals	-0.12	0.29	-4.2E-03	0.02	0.35

Temporal trend statistics for suspended sediment concentration - discharge and water yield - precipitation relationships in the lower Salinas River. Fine sediment is defined as particles with a diameter (D) < 62.5  $\mu\text{m}$ . Sand is defined as  $62.5 \leq D \leq 2000 \mu\text{m}$ . LR = linear regression,  $C_{SSf}$  = fine suspended sediment concentration,  $C_{SSs}$  = sand suspended sediment concentration,  $Q$  = discharge,  $Wy$  = water yield,  $P$  = precipitation.

## Figure Captions

**Figure 1.** The Salinas River watershed. The locations of U.S. Geological Survey (USGS) hydrologic gauging stations are marked with dotted circles and identification codes. Identification codes S1 and S2 correspond to gauge names: *Salinas R. near Spreckels* and *Salinas River near Chualar* (USGS gauge numbers 11152500 and 11152300), respectively. The Davis Street Bridge suspended sediment sampling location is indicated by a line. The National Oceanographic and Atmospheric Administration precipitation gauge 'Big Sur State Park' is indicated with a black triangle and the label BGS.

**Figure 2.** Linear regression (LR) and LOESS rating curve models for suspended sediment concentration – water discharge behavior in log-log space for (a) fine sediment and (b) sand sized sediment over the sampling period (1967 – 2011). Water yield – precipitation relationships are similarly modeled with linear regression and LOESS techniques for the entire period of S1 discharge measurement (c) 1931 – 2011, and the suspended sediment sampling period (d) 1967 – 2011.

**Figure 3.** Plots of (a) fine sediment and (f) sand LOESS residuals sequentially summed over time. (b-d, g-i) Arrayed beneath each sediment class are the sequential sums of the mean corrected hydrologic variables found to exert significant control at the event to

inter-annual scale, and (e,j) the daily discharge hydrograph at gauge S1. Gray shading indicates zones of persistent low residual values, un-shaded zones are positive, and relatively stable periods are highlighted with light blue bars. The dates of the three highest discharge events during the suspended sediment record are indicated on the (e) hydrograph.

**Figure 4.** El Niño and lower Salinas discharge events: (a) Oceanic Niño Index (ONI) plotted as a 3 month running mean of sea surface temperature anomaly in the Nino 3.4 region; (b,c,d,e) The number of days when daily discharge ( $Q_d$ ) was  $\geq 400$ ,  $200$ ,  $100$ ,  $1 \text{ m}^3\text{s}^{-1}$ , or  $\leq 0.1 \text{ m}^3\text{s}^{-1}$  respectively, by water year. Plot (a) is offset to accommodate the water year abscissa for plots (b) through (e). Shaded zones mark strong to moderate El Niño years, with upper years in plot (a) identifying strong El Niño years and lower years indicating strong La Niña years.

**Figure 5.** The lower Salinas River gauge S1 annual sum of days with daily discharge greater than or equal to a) 400, b) 200, c) 100, d)  $1 \text{ m}^3\text{s}^{-1}$ , e) less than or equal to  $0.1 \text{ m}^3\text{s}^{-1}$  vs, and f). annual precipitation at the NOAA Big Sur State Park (BGS) gauge vs. peak annual Ocean Niño Index (ONI).

**Figure 6.** (a, b) Fine suspended sediment and (c, d) sand sized suspended sediment (a, c) log linear regression residuals and (b, d) LOESS  $C_{ss} \sim Q$  residuals plotted over time with fitted linear temporal trend estimations.

**Figure 7.** Water yield ~ precipitation residuals (a, b) plotted over the period of discharge measurement at S1 on the lower Salinas River (1930-2011), and (c, d) the period of record for suspended sediment (1967-2011). Residuals were derived from (a, c) linear regression, and (b, d) LOESS curves.

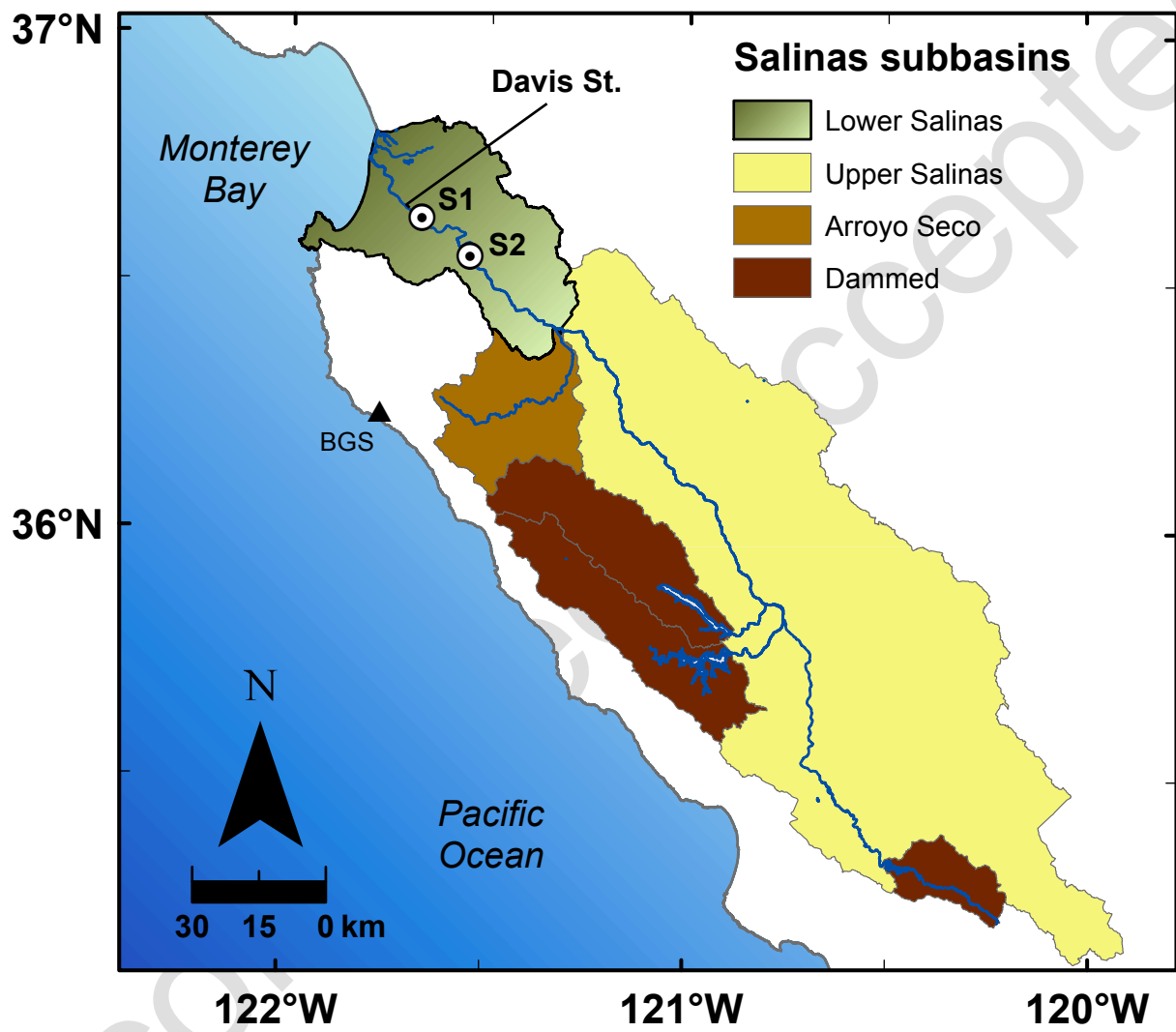


**Figure 1.**

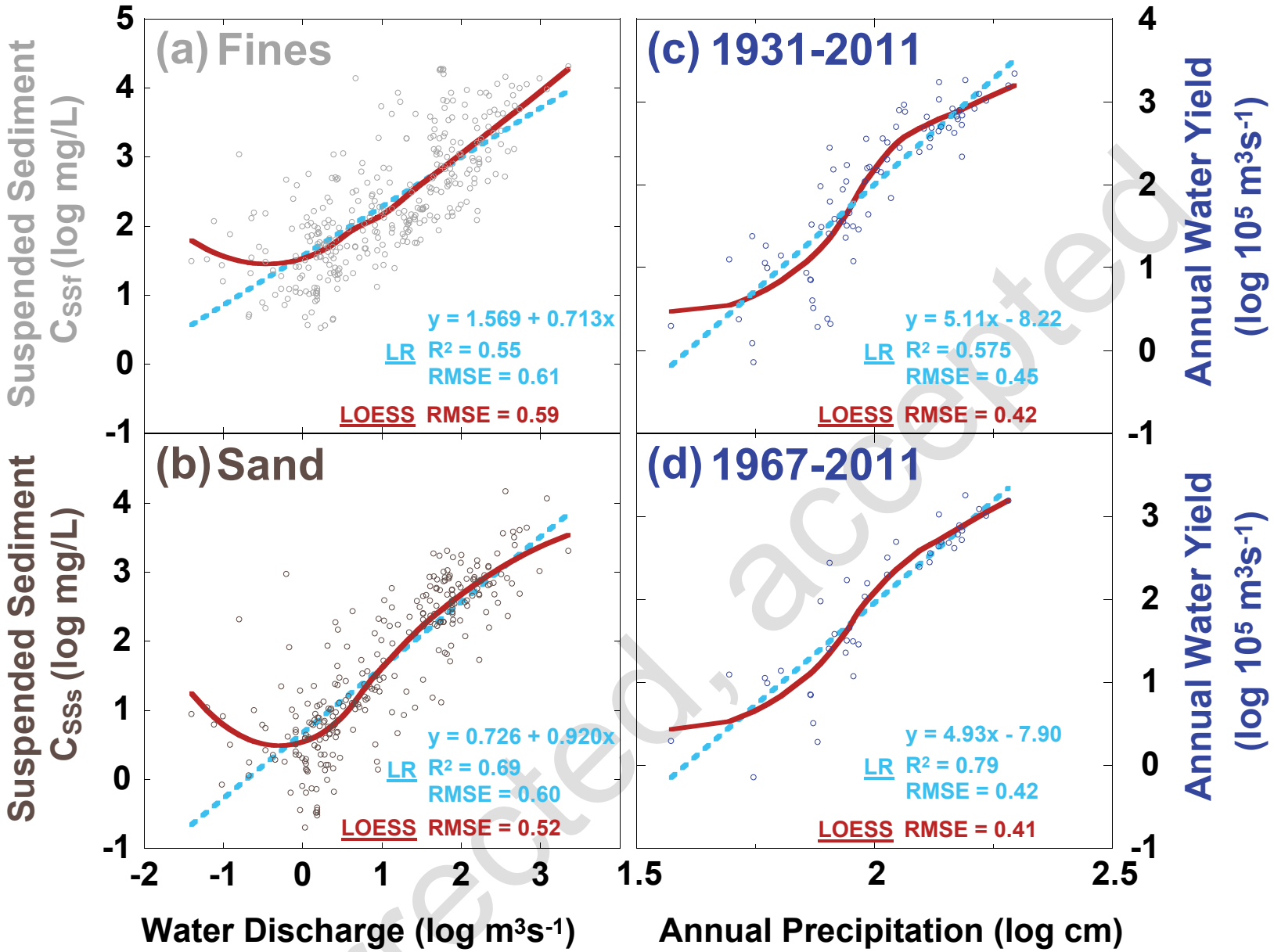


Figure 2.

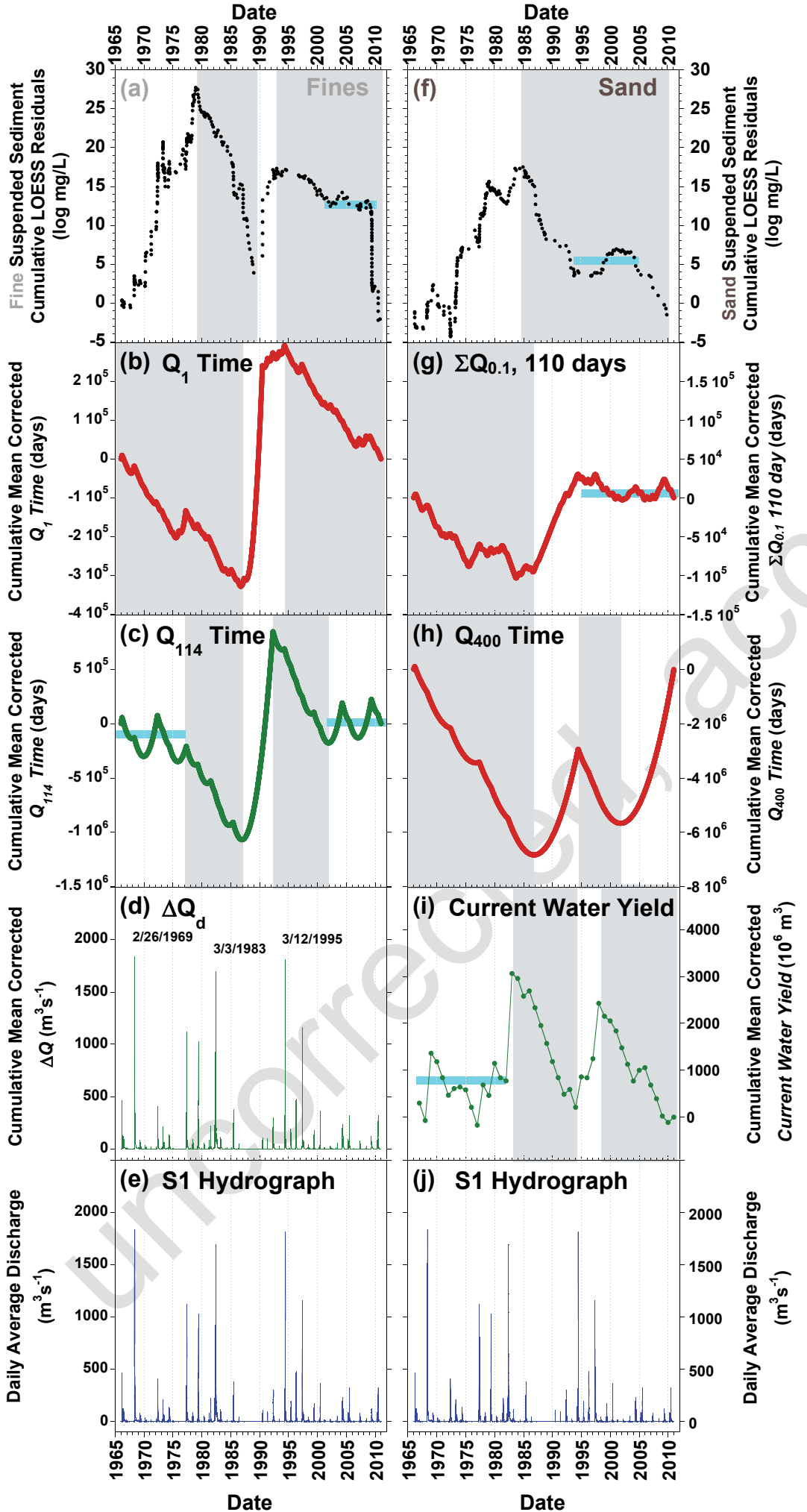


Figure 3.

# Oceanic Nino Index

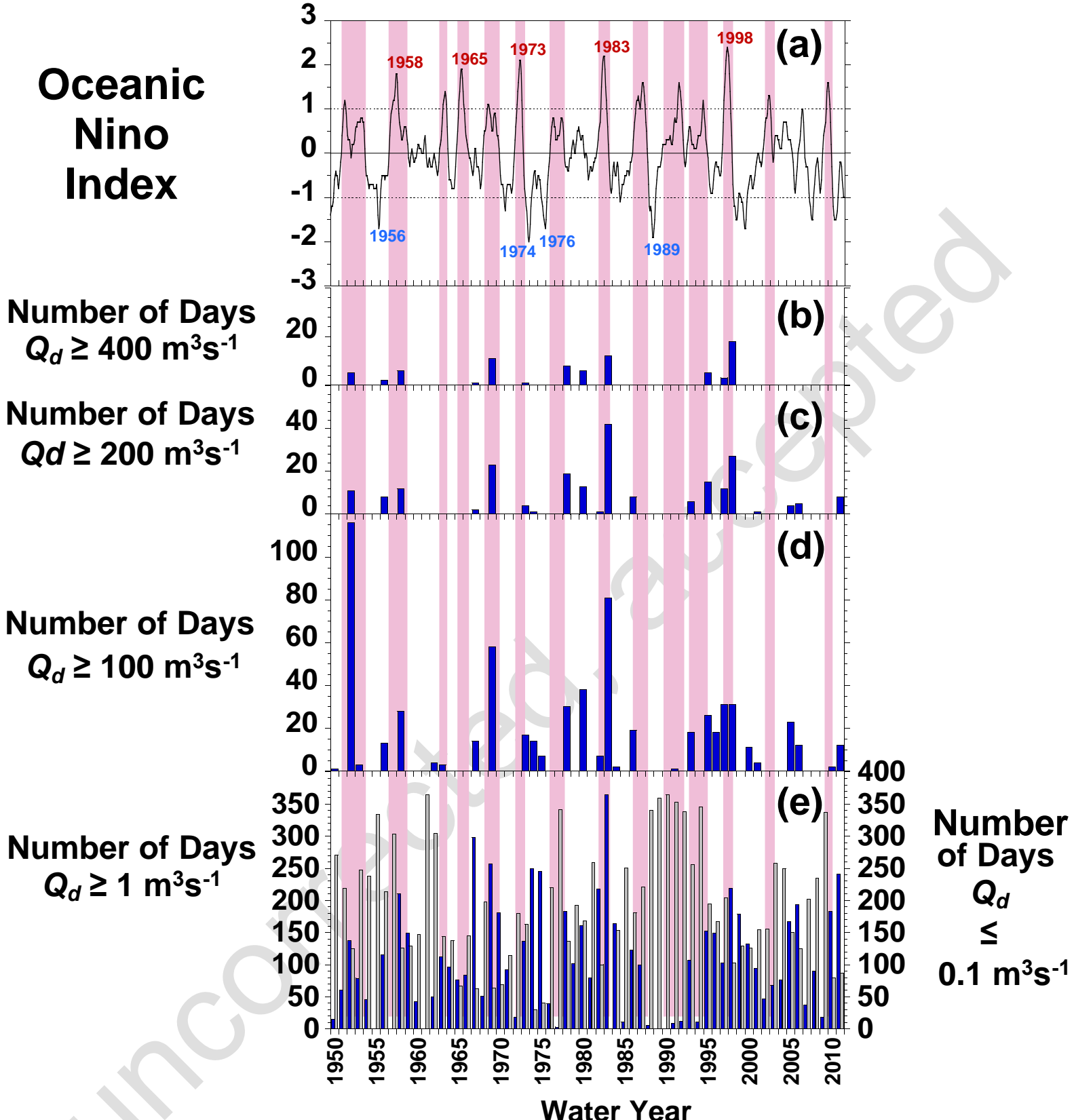


Figure 4.

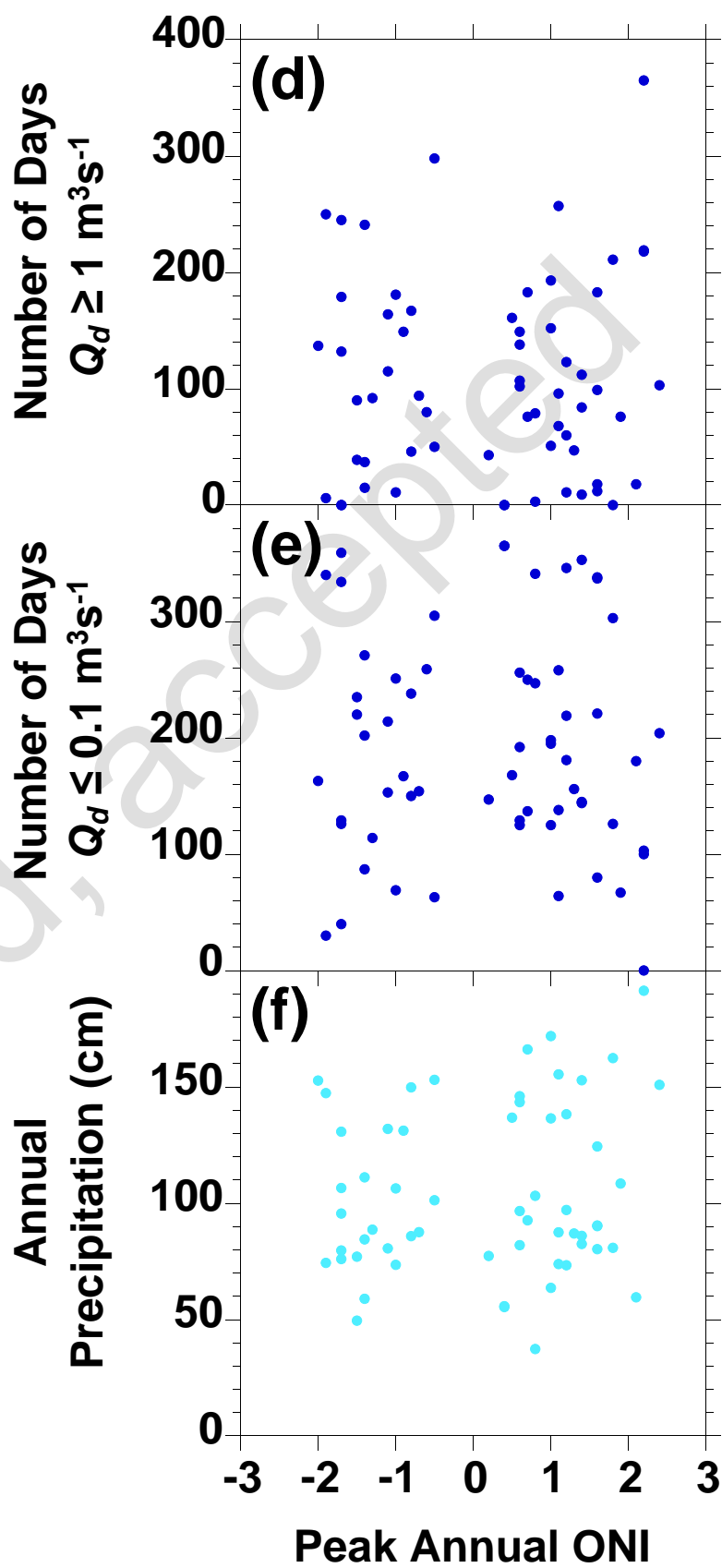
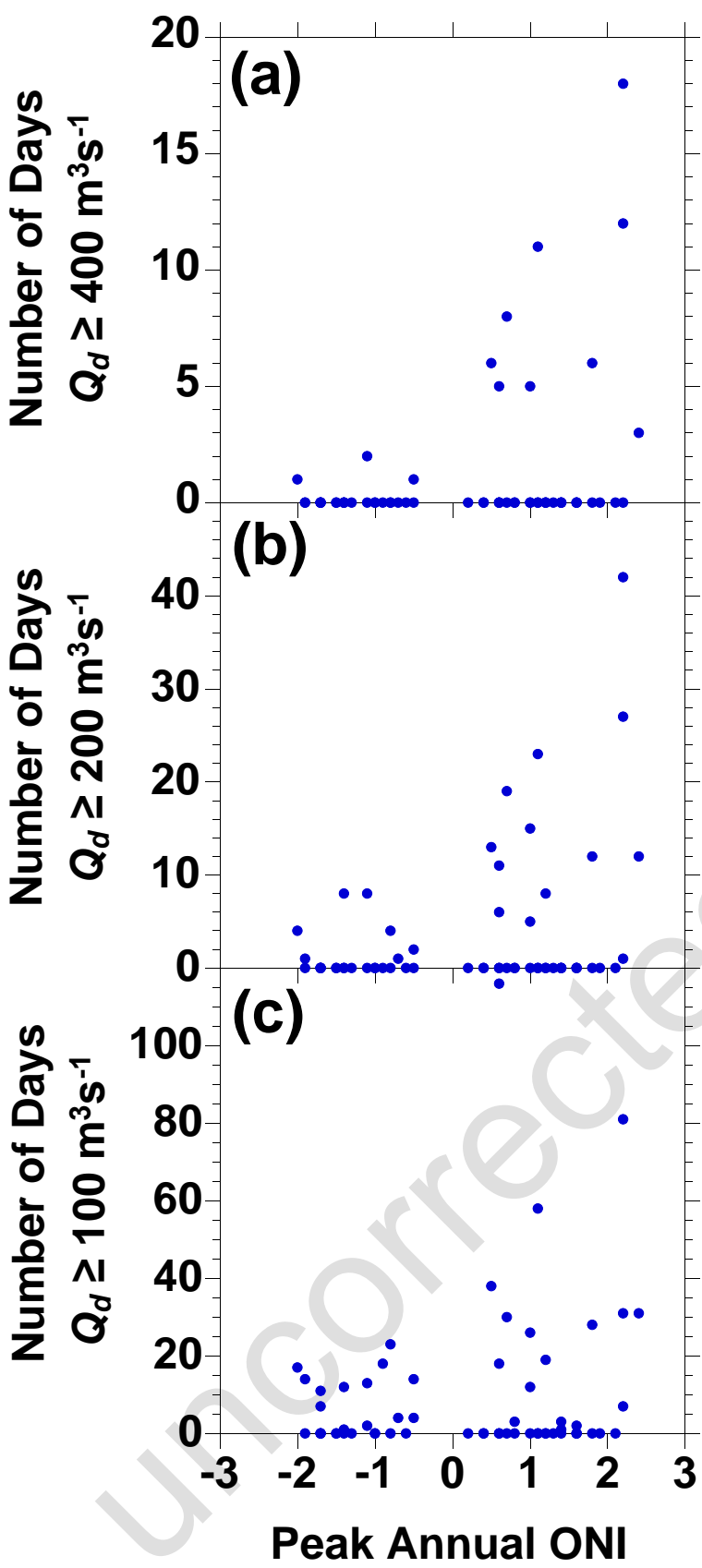


Figure 5.

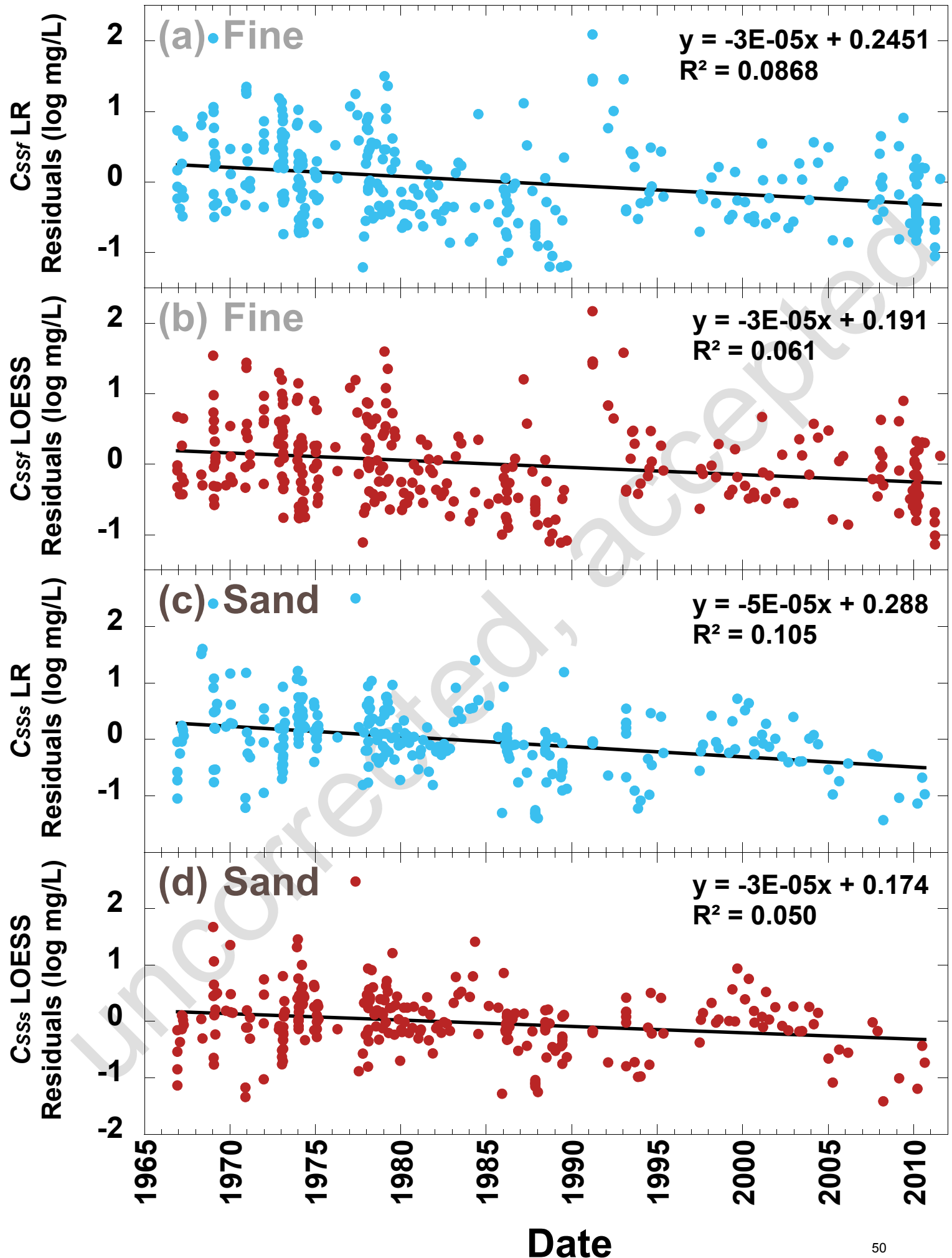


Figure 6.

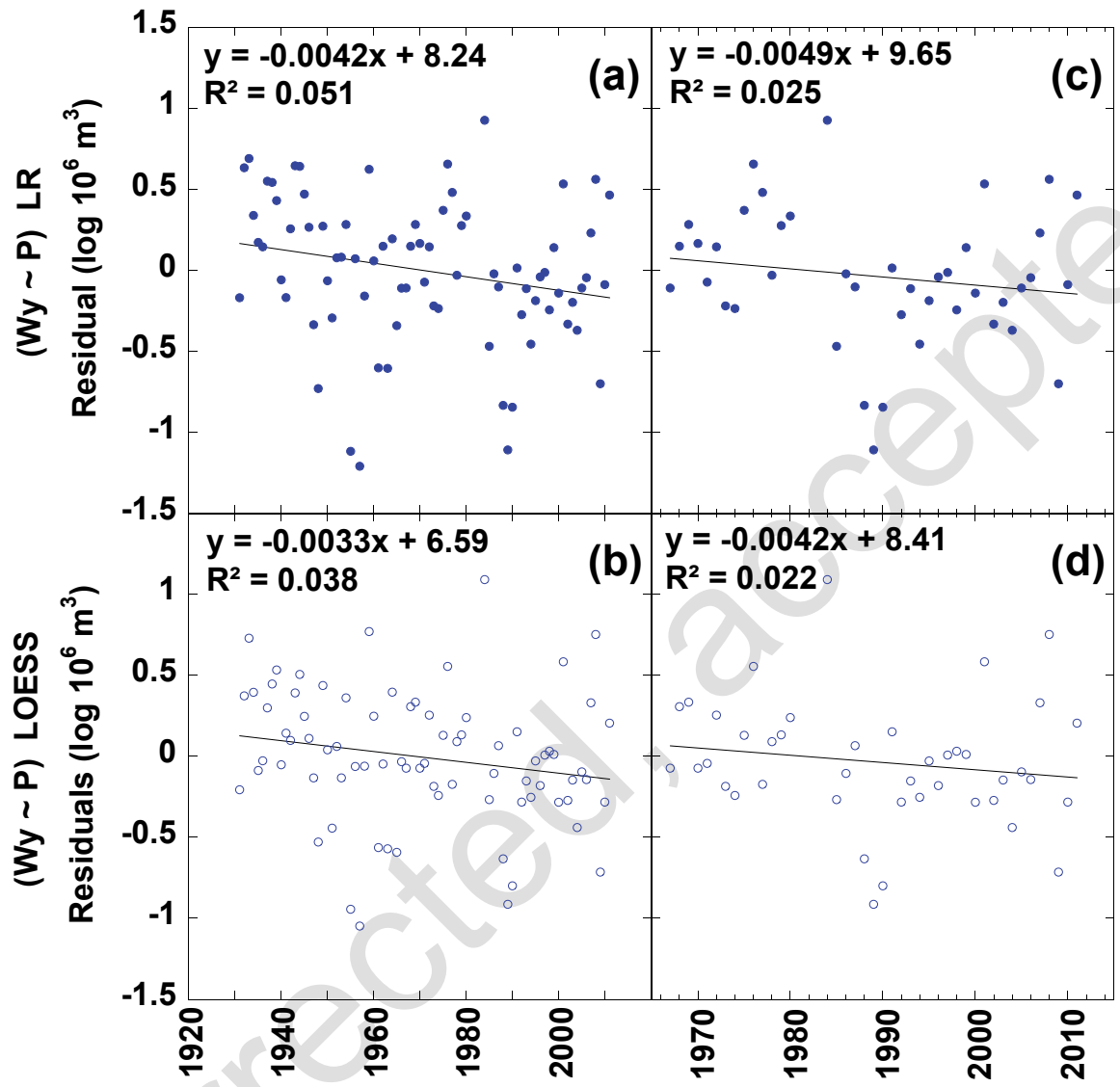


Figure 7.